

Compact mid-IR sources east of galactic center source IRS5

M. Perger¹, J. Moultağa^{1,2}, A. Eckart^{1,3}, T. Viehmann¹, R. Schödel¹ and K. Muzic^{1,3}

¹ I. Physikalisches Institut, Universität zu Köln, Zülpicher Str. 77, 50937 Köln, Germany

² Laboratoire d'Astrophysique de Toulouse, UMR 5572, Observatoire Midi-Pyrénées, 14 avenue Edouard Belin, 31400 Toulouse, France

³ Max-Planck-Institut für Radioastronomie, Auf dem Hügel 69, 53121 Bonn, Germany

Received 9. Aug. 2007 / Accepted 25. Oct. 2007

ABSTRACT

Aims. Mid-infrared observations of the Galactic Center show among the extended mini-spiral a number of compact sources. Their nature is of interest because they represent an interaction of luminous stars with the mini-spiral material or mass losing sources that are enshrouded in dust and gas shells. Characterizing their nature is necessary in order to obtain a complete picture of the different stellar populations and the star formation history of the central stellar cluster in general. Prominent compact MIR sources in the Galactic Center are either clearly offset from the mini-spiral (e.g. the M2 super-giant IRS 7 and the bright dust enshrouded IRS 3) or have been identified earlier with bright bow shock sources (e.g. IRS 21, 1W, 10W and IRS 5). There are, however, four less prominent compact sources east of IRS 5, the natures of which were unclear until now.

Methods. We present near-infrared K-band long slit spectroscopy of the four sources east of IRS 5 obtained with the ISAAC spectrograph at the ESO VLT in July 2005. We interpret the data in combination with high angular resolution NIR and MIR images obtained with ISAAC and NACO at the ESO VLT.

Results. The K'-band images and proper motions show that the sources are multiple. For all but one source we find dominant contributions from late type stars with best overall fits to template stars with temperatures below 5000 K.

Conclusions. The brightest sources contained in IRS 5NE, 5E and 5S may be asymptotic giant branch stars and a part of the MIR excess may be due to dust shells produced by the individual sources. However, in all cases an interaction with the mini-spiral cannot be excluded and their broad band infrared SEDs indicate that they could be lower luminosity counterparts of the identified bow shock sources. In fact, IRS 5SE is associated with a faint bow shock and its spectrum shows contributions from a hotter early type star which supports such a classification.

Key words. Galaxy: center - galaxies: nuclei - infrared: ISM extinction

1. Introduction

The Galactic Center (GC) at a distance of ~ 8 kpc (Ghez et al. 2005; Schödel et al. 2002, 2003; Eisenhauer 2003, 2005) is known as a bright source of near- and mid-infrared (NIR and MIR) radiation since the late 1960s ((Becklin & Neugebauer 1968); (1969); (Low et al. 1969)). The main source of NIR radiation is photospheric emission from a dense stellar cluster, i.e. a crowded field of point sources, while almost all of the MIR radiation originates from extended gas and dust features as well as dust emission from the circum-stellar regions of a dozen individual sources interacting with the more extended GC interstellar medium (ISM).

The GC stellar cluster shows some intriguing characteristics: it is extremely dense, with an unusual observed stellar population ((Genzel et al. 2003); (Eisenhauer et al. 2005)). Recently, Schödel et al. (2007) presented AO assisted high-resolution NIR imaging observations of the stellar cluster within $20''$ (about 0.75 pc) of Sgr A*, the massive black hole at the center of the Milky Way. Schödel et al. (2007) extracted stellar number counts and colors, and derived from them the detailed structure of the nuclear stellar cluster and an extinction map across it. The bright members of the central stellar cluster are mainly (80% of all $m_K \leq 14$ mag stars; (Ott et al. 1999)) late-type red giants (e.g. IRS 7 and IRS 10E in Fig. 1), many of which

are suspected to lie on the asymptotic giant branch (AGB). It is also composed of young massive stars which have energetic winds (e.g. (Krabbe et al. 1995); (Najarro et al. 1997); IRS 13E in Fig. 1) and are arranged in two stellar disks ((Genzel et al. 2003); (Paumard et al. 2006)). Spectra of AGB stars show strong $2.3 \mu\text{m}$ CO bandhead absorption and the massive, hot and windy stars (He-stars) exhibit He/H emission. These emission line stars dominate the NIR luminosity of the central few arcseconds. All bright and compact MIR sources in the GC are either clearly offset from the mini-spiral (such as the M2 super-giant IRS 7 and the bright dust enshrouded IRS 3) or have been identified earlier with bright bow shock sources (like IRS 21, 1W, 10W and IRS 5).

A third, less numerous component of the GC stellar cluster, consists of luminous objects with steep, red and featureless (K-band-) spectra and a strong infrared excess. Although clearly extended in MIR images they are quite compact in this wavelength range compared to the mini-spiral or the dust shell around IRS 3 ((Viehmann et al. 2006)). These clearly extended dust embedded MIR sources (e.g. IRS 5, 10W in Fig. 1) are bow shock sources, caused by bright emission-line stars with strong winds plowing through the ambient gas and dust of the northern arm of the mini-spiral ((Tanner et al. 2002); (2003); (2005); (Rigaut et al. 2003); (Geballe et al. 2004); (Geballe et al. 2006)). There are also fainter dust embedded sources (e.g. the IRS 13N cluster in Fig. 1; (Eckart et al. 2004)) which could represent a low luminosity class of bow shock sources or even young dust embedded

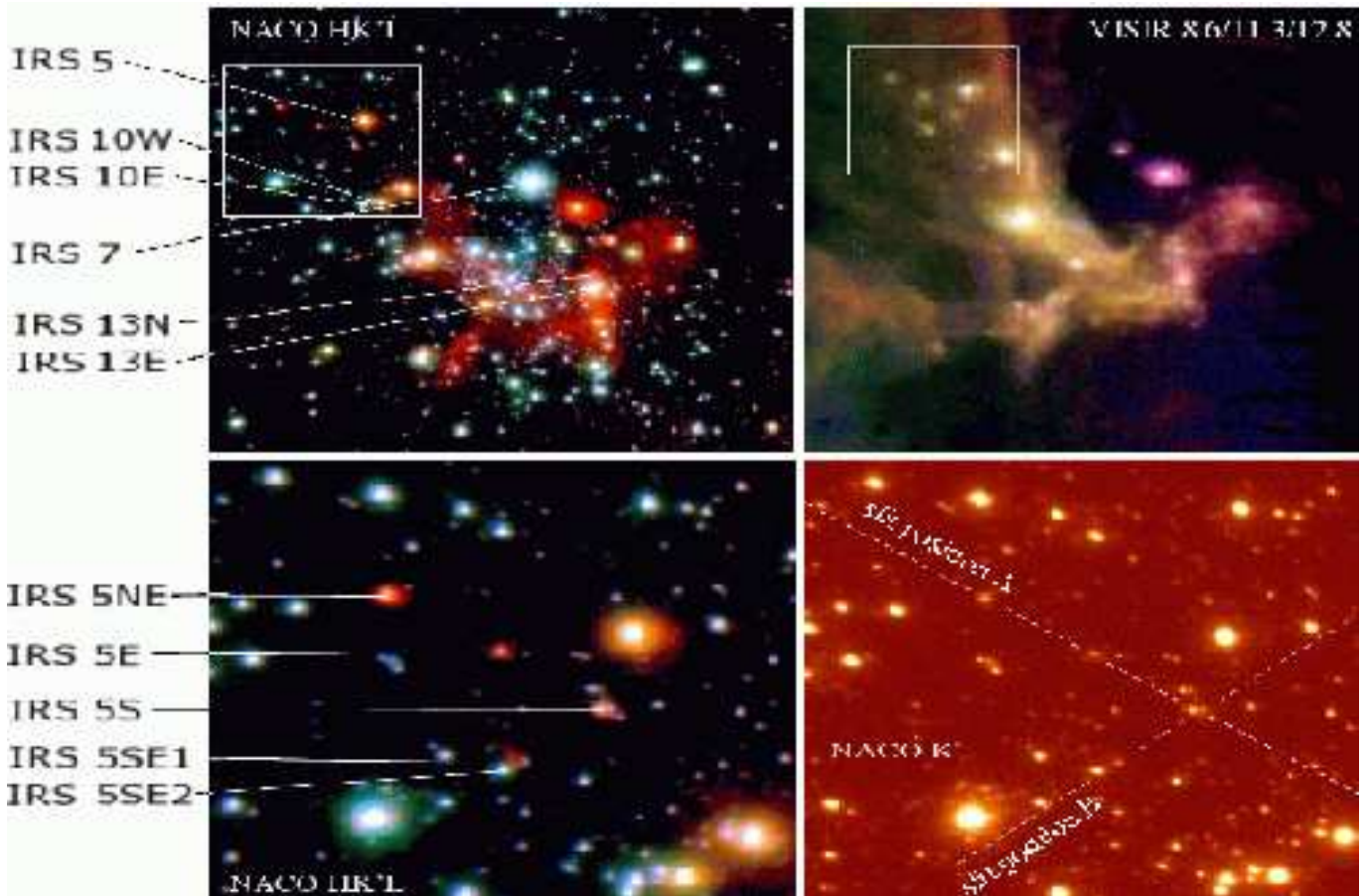


Fig. 1. Upper left: NACO HK'L-image of the inner $30'' \times 30''$ region of the GC. Upper right: VISIR N-band three-color composite view of the GC. The blue channel is $8.6 \mu\text{m}$, green is $11.3 \mu\text{m}$, and red is $12.8 \mu\text{m}$ ($30'' \times 30''$). Lower left: NACO HK'L-image of the observed sources ($6'' \times 6''$). A more detailed nomenclature of sources is given in Table 1 and Fig. 3. Lower right: NACO K'-band image of the observed sources ($6'' \times 6''$). The white insets in the top panels indicate the location of the enlarged area shown in the lower panels. The dashed white lines in the lower right panel indicate the orientation of the $0.6''$ ISAAC slits.

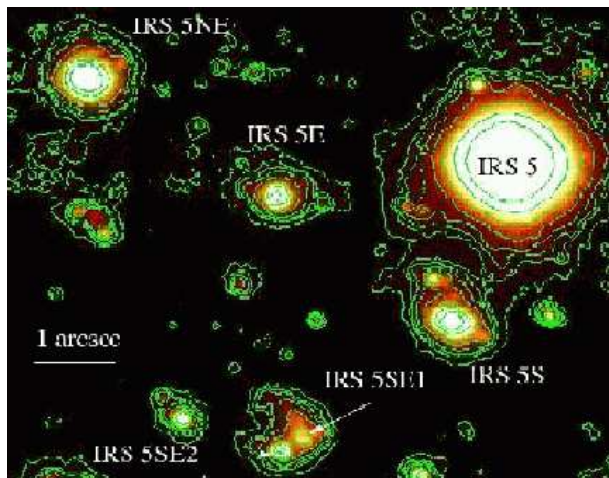


Fig. 2. An L'-band shift-and-add adaptive optics image showing the compact MIR sources east of IRS 5 with logarithmic contours. The extended bow shock like structure to the northeast of IRS 5SE1 is clearly visible.

stars that have been recently formed. In this paper we investigate compact MIR sources close to or within the northern arm of the mini-spiral.

Infrared images longward of $2 \mu\text{m}$ show four bright compact objects ((Viehmman et al. 2006)) located to the east of the bright northern arm source IRS 5. They are especially prominent in high angular resolution MIR images as obtained with VISIR (see Fig. 1 and a zoom towards the described sources in Fig. 2). These sources have an exceptional appearance since they are quite compact compared to the bulk of the $10 \mu\text{m}$ emission which is associated with the extended mini-spiral. The nature of these four compact sources, which we refer to as IRS 5NE, 5E, 5S and 5SE (see Fig. 1; IRS 5SE includes 5SE1 and 5SE2), is currently unclear: they are almost as bright as IRS 7 (M2 supergiant in Fig. 1; (Carr et al. 2000)) in the N-band, while they appear much less prominent (but still detectable) at shorter wavelengths (K-band), although they remain bright in L- and M-bands. We present first high angular resolution images, proper motions and K-band long-slit spectroscopy as obtained with the ESO VLT, in order to further investigate the properties of these sources.

2. Observations and data reduction

2.1. Proper motion data

The K'-band ($2.18 \mu\text{m}$) images from which we derived the proper motions of the sources were taken

with the NAOS/CONICA¹ adaptive optics assisted imager/spectrometer ((Lenzen et al. 1998); (Rousset et al. 1998); (Brandner et al. 2002) at the UT4 (YEPUN) at the ESO² VLT³, Cerro Paranal, Chile. The data set includes the images from epochs 2002.339, 2003.356, 2004.512, 2004.521 and 2006.413⁴ with an angular resolution of ~ 56 mas. Data reduction (bad pixel correction, sky subtraction, flat field correction) and formation of final mosaics was performed using the DPUSER software for astronomical image analysis (T. Ott; see also (Eckart et al. 1990)). The absolute positions of sources in our AO images were derived by comparison to the VLA positions of IRS 10EE, 28, 9, 12N, 17, 7 and 15NE as given by (Menten et al. 1997) and (Reid et al. 2003) (for identification of different GC sources see e.g. Fig. 2 in (Viehmann et al. 2005)). The radio positions and the positions in the K'-band image agree to within less than a single 27 mas pixel i.e. less than a K'-band diffraction limited beam. The stars used for the transformation were chosen to be uniformly distributed across the field. In addition to the MIR excess sources east of IRS 5 we have randomly selected 27 objects in the field for comparison. The positions and K'-band proper motions of all sources are listed in Table 1 and shown in Figs. 3 and 4. The proper motions of the overall source sample in Table 1 are in agreement with random motions. Within the width of the velocity distributions of about $\sigma_{field}=150$ km/s their median velocities of about -63 km/s to the east and 2 km/s to the north are close to zero with random orientations.

2.2. ISAAC observations

On July 27th and 28th 2005⁵, K-band (2.2 μm) spectroscopy observations of the four MIR sources east of IRS 5 ($m_{K,obs} \sim 8$ to 11 mag) were obtained with the ISAAC⁶ infrared spectrometer mounted at the UT1 (ANTU) at the ESO VLT. The seeing-limited spectra (0.7 to 1.6'') were taken with a long-slit of 0.6 x 120'' (two slit positions A and B, see Fig. 1) in ISAAC's lower resolution mode ($R=\lambda/\Delta\lambda=840$). The observations were made with an integration time of 100 sec per frame with total integration times of 2400 sec for IRS 5S and 1200 sec for the remaining 3 objects IRS 5NE, 5SE, and 5E.

The spectroscopy data reduction was carried out with IRAF⁷ & IDL⁸ using standard procedures: the sky-subtraction was achieved with a nodding technique and flat-fielding was applied. The individual spectra were corrected for slit-curvature and shifts. Creating a median of individual spectra then resulted in the final spectrum for a given source. Telluric correction was performed with A- and B-type stars, the observations of which directly followed or preceded those of the targets. The hydrogen absorption line (B γ at 2.17 μm) in the stellar template spectra was removed by fitting a Lorentz-profile to the line prior to the

Table 1. Proper motion data (and their 1σ uncertainties) of the compact IRS 5 N-band sources derived from NACO K'-band data, covering the epochs 2002.339, 2003.356, 2004.512, 2004.521 and 2006.413 with a resolution of ~ 56 mas. Positive velocities go from west to east and south to north. The epoch 2002 K'-band positions are referred to SgrA* with a 1σ uncertainty of 0.1''

Source	Δ_α [']	Δ_δ [']	$v_{R.A.}$ [km/s]	v_{Dec} [km/s]
IRS 5	9.31	9.15	43 \pm 18	-27 \pm 12
IRS 5NE1	13.79	9.60	-156 \pm 34	82 \pm 20
IRS 5NE2	13.31	9.88	-346 \pm 10	279 \pm 12
IRS 5E1	11.68	8.50	-48 \pm 30	183 \pm 25
IRS 5E2	13.31	9.88	-299 \pm 10	216 \pm 12
IRS 5S1	9.80	7.31	105 \pm 14	2 \pm 13
IRS 5S2	9.62	7.32	102 \pm 14	-34 \pm 16
IRS 5S3	9.42	7.19	179 \pm 22	-46 \pm 16
IRS 5SE1	10.00	6.06	60 \pm 19	-22 \pm 16
IRS 5SE2	11.30	5.91	-150 \pm 10	24 \pm 10
# 1	7.82	9.42	-113 \pm 10	-69 \pm 11
# 2	8.75	7.52	28 \pm 9	-26 \pm 10
# 3	7.22	7.50	-20 \pm 12	-96 \pm 12
# 4	6.87	8.70	-102 \pm 11	-181 \pm 11
# 5	6.45	6.50	-112 \pm 15	45 \pm 16
# 6	8.25	5.20	-299 \pm 52	79 \pm 25
# 7	9.98	5.80	69 \pm 9	-46 \pm 10
# 8	11.27	5.21	9 \pm 22	-5 \pm 16
# 9	9.90	4.20	-17 \pm 9	106 \pm 11
# 10	12.47	6.11	-247 \pm 8	48 \pm 10
# 11	11.18	7.19	-96 \pm 10	-170 \pm 12
# 12	10.30	8.62	18 \pm 9	228 \pm 10
# 13	12.05	9.87	-263 \pm 10	222 \pm 12
# 14a	13.80	8.22	-308 \pm 16	322 \pm 15
# 14b	13.67	8.23	-210 \pm 20	127 \pm 18
# 14c	13.67	8.08	-139 \pm 32	304 \pm 24
# 14d	13.46	8.12	-46 \pm 49	64 \pm 32
# 14e	13.40	8.00	-334 \pm 10	65 \pm 11
# 15	9.79	9.92	79 \pm 9	-50 \pm 10
# 16	11.93	11.20	-50 \pm 8	3 \pm 10
# 17	8.93	11.10	-63 \pm 14	-161 \pm 15
# 18	6.62	11.05	109 \pm 11	-9 \pm 11
# 19	7.93	6.00	14 \pm 10	45 \pm 11
# 20	12.32	5.04	-165 \pm 10	218 \pm 11
# 21a	10.00	7.83	-69 \pm 13	-14 \pm 13
# 21b	9.87	7.82	-102 \pm 23	-157 \pm 17
# 21c	9.75	7.62	-53 \pm 12	-111 \pm 12

telluric correction. At wavelengths of less than 2 μm we used the underlying black body continuum of the star. Consequently no line correction was applied. After division by the spectrum of the telluric standards, the spectra of the four MIR sources east of IRS 5 were multiplied by a blackbody of temperature equal to the effective temperature of the standard stars. The spectra were wavelength calibrated using Xenon-lines from additionally observed data frames. Flux density calibration was applied with zero points from literature ($FD_{0,K} = 657$ Jy, (Skinner 1997)) and high resolution NACO images (compared to IRS 16NE and 16NW). Strong atmospheric CO₂ absorption result in lower signal-to-noise ratios (SNRs) in the 1.98 to 2.06 μm spectral regions. At shorter wavelengths the SNR of the spectra suffer from residual telluric H₂O absorption and the strong (~ 30 mag; see below) extinction towards the GC region.

¹ Nasmyth Adaptive Optics System/COude Near Infrared Camera; (Lenzen et al. 2003); (Rousset et al. 2003)

² European Southern Observatory

³ Very Large Telescope

⁴ ESO program IDs: 60.A-9026(A), 073.B-0775(A,B), 077.B-0552(A)

⁵ ESO program ID: 075.C-0138(A)

⁶ Infrared Spectrometer And Array Camera, (Moorwood et al. 1998)

⁷ Image Reduction and Analysis Facility, distributed by the National Optical Astronomy Observatory (NOAO), operated by the Association of Universities for Research in Astronomy, Inc. (AURA) and under cooperative agreement with the National Science Foundation (NSF)

⁸ Interactive Data Language

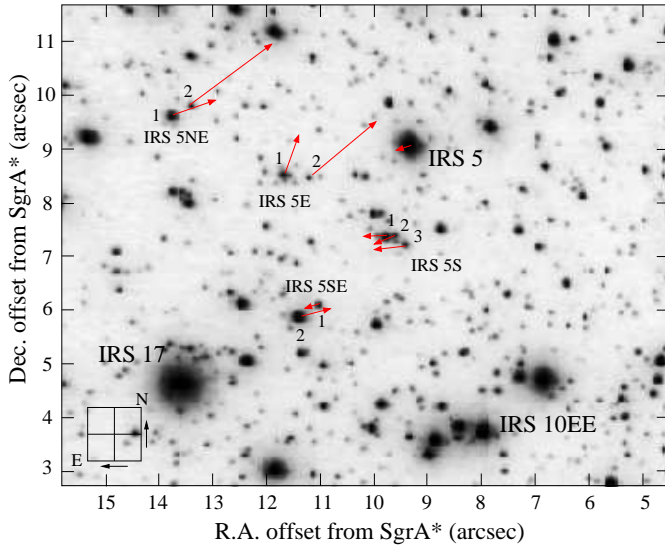


Fig. 3. Proper motions of the compact MIR excess sources east of the northern arm of the mini-spiral.

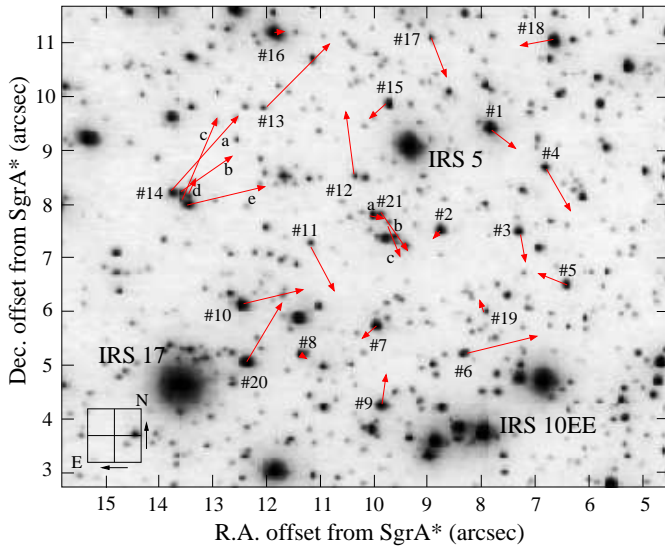


Fig. 4. Proper motions of randomly selected sources to the east of IRS 5. In both panels (Figs. 3 and 4) the square in the lower left corner indicates the orientation of positive velocity vectors and has a total width of 200 km/s in both directions.

3. Results

3.1. Structures and proper motions of individual sources

In this section we discuss the structures and proper motions of the individual compact MIR sources east of IRS 5 as obtained from our high angular resolution K' -images.

IRS 5NE: The K' -band images show two sources with a separation of $0.4''$. Both sources are moving towards the northwest but their velocity difference is large with respect to the uncertainties and σ_{field} . This implies that the two sources are not physically associated.

IRS 5E: The situation is similar to that of IRS 5NE. IRS 5E1 and IRS 5E2 are an apparent double source with an east-west separation of $0.5''$ and a large proper motion velocity difference. IRS 5E2 is about half as bright as IRS 5E1. Both sources are moving towards the northwest. The images also indicate several sources which are at least 1 magnitude fainter than IRS 5E1 and

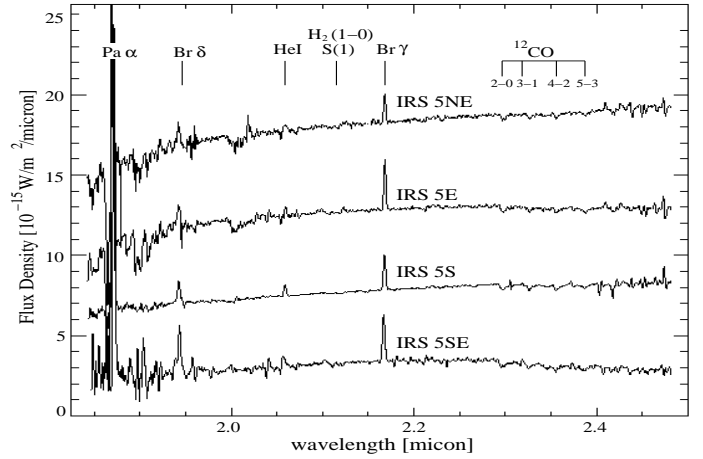


Fig. 5. The fully reduced spectra of IRS 5NE, 5E, 5S and 5SE. The most prominent absorption and emission lines are marked. The flux densities are shifted for display purposes (IRS 5NE: $+15 \times 10^{-15} \text{ W/m}^2/\mu\text{m}$, 5E: $+10 \times 10^{-15} \text{ W/m}^2/\mu\text{m}$, 5S: $+5 \times 10^{-15} \text{ W/m}^2/\mu\text{m}$, 5SE: $-5 \times 10^{-15} \text{ W/m}^2/\mu\text{m}$). Note the lower SNR for wavelengths smaller than $1.94 \mu\text{m}$ and at around $2.02 \mu\text{m}$. For spectral flux calibration - see 2.2.

have separations of less than $0.5''$ from it. They are too faint to determine their proper motions.

IRS 5S: Here a minimum of 3 sources within a $0.6''$ diameter region is moving towards the east-southeast. Their proper motion velocity difference is small with respect to the uncertainties and σ_{field} . This implies that these sources could be physically associated. A firm statement on this requires a determination of their radial velocities in the near future.

IRS 5SE: High-resolution NAOS/CONICA K' - and L-band images (see Fig. 1) reveal that the southernmost of the four sources, which appears slightly extended ($\approx 0.2''$; compared to IRS7) in the VISIR images, is in fact an apparent double source, consisting of a 'blue' point source to the east (SE2) and a fainter point source to the west (SE1). The spectrum we obtained from IRS 5SE probably includes flux density contributions from both objects. We calculated a separation between the two objects as $0.4 \pm 0.1''$. Their proper motion velocity difference is large with respect to the uncertainties and σ_{field} . This implies that the two sources are not physically associated. IRS5 SE1 shows a tail like structure (in the L'-band) that appears to be the main source of emission at longer wavelengths. The extended dust feature has the appearance of a bow-shock. Since IRS5 SE2 is blue and bright it may be associated with a luminous star that interacts with the surrounding ISM. The position angle of the bow shock with respect to the proper motion of the source it is physically associated with, depends on the geometry and density structure of the local ISM it is moving in. Here offsets by $\sim 45^\circ$ appear to be possible (see Fig. 2).

3.2. Stellar types

To derive the stellar types of the observed sources we compared the reduced spectra shown in Fig. 5 with standard star templates from (Wallace & Hinkle 1997) of spectral types from O- to M- and different luminosity classes. Since the template spectra are continuum normalized to one, we had to multiply them by a blackbody of temperature equal to the effective temperature of each stellar type. The spectra were also convolved with a Gaussian distribution to match the resolution of our observed

Table 2. Extinction corrected flux densities (FD) of the compact N-band sources in Janskys ((Viehmann et al. 2006)) and H-, K- and L-band flux densities and magnitudes (m) from NACO high resolution images (compared to IRS 16NE and 16NW). Errors are around 30% for sources of more than 0.5 Jy and 50% for the sources with flux densities below that value. The H-, K- and L-band values have errors up to 75%. For the calculations, zero flux densities from Skinner et al. (2997) were used ($FD_{0,H} = 1020$ Jy, $FD_{0,K} = 657$ Jy, $FD_{0,L} = 253$ Jy). The colors H-K and K-L are shown.

Name	m_H	m_K	m_L	H-K	K-L	$FD_{1.6\mu m}$	$FD_{2.1\mu m}$	$FD_{3.8\mu m}$	$FD_{4.7\mu m}$	$FD_{8.6\mu m}$	$FD_{11.3\mu m}$	$FD_{12.8\mu m}$	$FD_{18.7\mu m}$	$FD_{19.5\mu m}$
IRS 5	–	–	4.4	–	–	–	–	4.270	4.880	5.110	4.210	5.850	3.210	2.850
IRS 5NE	14.8	12.7	9.5	2.1	3.2	0.001	0.006	0.047	0.800	0.510	0.600	0.560	0.950	0.740
IRS 5E	14.6	13.0	10.7	1.6	2.3	0.002	0.004	0.016	0.210	0.590	1.060	1.540	1.580	1.720
IRS 5S	14.3	12.4	9.9	1.8	2.5	0.002	0.007	0.032	0.430	0.630	0.510	0.380	0.630	1.060
IRS 5SE1	–	–	12.1	–	–	–	–	0.004	0.180	0.500	0.970	1.100	2.840	3.580
IRS 5SE2	13.2	11.6	10.5	1.7	1.0	0.005	0.016	0.018	–	0.040	0.090	0.130	–	–
IRS 13N	13.0	12.4	10.0	0.6	2.4	0.006	0.007	0.028	1.580	0.380	0.650	1.110	0.550	0.580

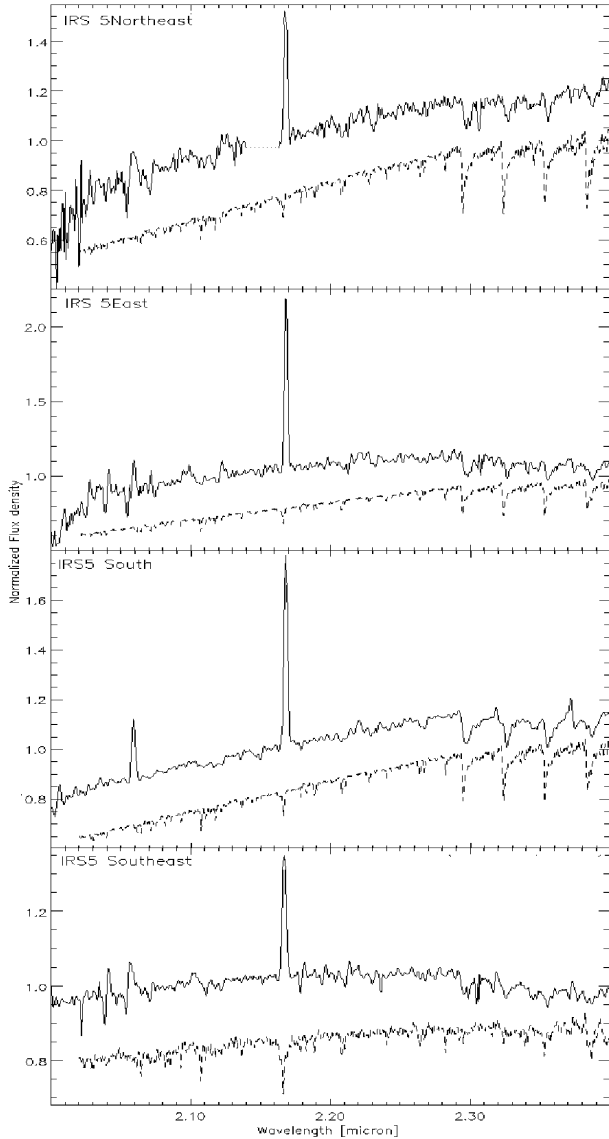


Fig. 6. Flux density normalized reduced spectra (upper curve) and flux density normalized and extinguished standard star spectra (lower curve) by Wallace & Hinkle (1997) which show the smallest differences in magnitude and in the CO bandhead depth and EW. The latter are shifted along the flux density axis for display purposes. For IRS 5SE the identification of a strong early type stellar contribution to the spectrum is also consistent with a reduced B_{ry} emission strength at the wavelength of the corresponding absorption in the template spectrum.

spectra.

The comparison was done by fitting the continuum of the source spectra (from 2.0 to 2.29 μm) with A_K extinguished template spectra, the apparent magnitude m_K , the depth d and the equivalent width (EW) of the ^{12}CO absorption bandheads. The fitting procedure is explained hereafter.

A small amount of apparent residual broadening of the CO bandheads may be due to the following fact: Most of the sources are apparently associated with small clusters of fainter stars. As the spectra are taken against the underlying stellar cluster in moderate seeing in a 0.6" diameter slit 4 to 6 sources that are individually up to 2 magnitudes fainter than the program source may lead to a systematic broadening of the order of the cluster velocity dispersion of $1\sigma \sim 150$ km/s (corresponding to a 3σ value of up to $\lambda/\Delta\lambda \sim 670 \sim 3\text{-}4$ nm at this position). In addition, the spectra are of lower SNR than those of the template stars. Since our fitting procedure is not solely based on the CO bandhead absorption, but also the extinction and apparent brightness of the objects, we consider the influence of these contamination effects to be negligible within the required accuracy of the procedure.

1. The visual extinction in the line of sight to the GC varies between 20 and 50 mag with an average of around 30 mag ((Rieke et al. 1989); see also the extinction map presented by (Schödel et al. 2007) and (Scoville et al. 2003)). It is mostly due to material along the line of sight to the GC, located, partly, in the the diffuse ISM ((Lebofsky 1979)) and partly, in the dense molecular clouds ((Gerakines et al. 1999)). In the K-band, the average extinction is $A_K = 0.112 \cdot A_V \approx 3.4$ mag ((Rieke & Lebofsky 1985); (Krabbe et al. 1995); (Scoville et al. 2003)).

In order to fit the observed spectra with those of template stars, we had to consider the foreground extinction. Therefore, we followed the same procedure as in Moultaqa et al. (2004) and applied the extinction law of Martin et al. (1990) to redden the template spectra. An extinguished spectrum is thus obtained as follows:

$$f_{ext,\lambda} = f_{0,\lambda} \cdot 10^{-0.4 \cdot A_K \cdot (2.2/\lambda)^{1.8}}$$

with $f_{ext,\lambda}$ and $f_{0,\lambda}$ as the extinct and intrinsic flux densities, respectively, and λ the wavelength in μm . The fitting process was done in the wavelength range from 2.07 to 2.29 μm , excluding the locations of detected prominent line features such as B_{ry} . We used this spectral range because it is mainly dominated by quasi-linear blackbody continuum and harbors no or few absorption and emission lines.

As a result of the unclear distribution of the K-band absorption due to the mini-spiral ((Schödel et al. 2007)), the fitting was done using K-band extinctions ranging from 2.4 to 4.4 magnitudes.

Table 3. Measured parameters of the observed and template spectra (taken from (Wallace & Hinkle 1997)) and physical parameters of the template stars.

Object	EW [nm]	d [nm]	m_K [mag]	Stellar Type	Temp. [K]
IRS 5NE	0.239	0.892	13.2	–	–
IRS 5E	0.365	0.849	13.6	–	–
IRS 5S	0.326	0.885	12.9	–	–
IRS 5SE	0.188	0.931	11.8	–	–
HR 2456	0.099	0.974	10.3	O7V	34600
HR 6165	0.028	0.966	11.4	B0V	28000
HR 5191	0.059	1.000	13.5	B3V	22570
HR 3323	0.146	0.904	13.3	G5III	4400
HR 3212	0.256	0.848	13.2	G7III	4286
HR 2985	0.283	0.834	13.2	G8III	4229
HR 6703	0.226	0.846	13.2	G8III	4229
HR 8317	0.516	0.755	12.9	K0III	4114
HR 8694	0.407	0.773	12.9	K0III	4114

2. The apparent K-band magnitudes of the standard stars at the distance of the GC ($r = 8000$ pc; (Eisenhauer et al. 2003)) are obtained via

$$m_K = M_K + 5 \cdot \log r - 5 \approx M_K + 14.52$$

where $M_K = M_V - (V-K)$. The absolute magnitudes and colors are taken from Lang (1992) and Allen (2000).

The apparent magnitudes of the template stars are compared to the extinction corrected K-band magnitudes of the observed sources shown in Tables 2 and 3.

3. All sources clearly show the rotational vibrational $^{12}\text{CO}(2-0)$ absorption bandhead at $2.2935 \mu\text{m}$. It is the strongest absorption feature in K-band and depends, among other parameters, on the temperature of the objects and is therefore a good tracer of spectral types.

Gaffney et al. (1993; 1995) show that the shape of this feature is fully characterized by its EW. Therefore, in the fitting process, the depth d and the EW of this absorption feature are also considered as parameters to be fitted. The CO 2-0 band head depth is proportional to $1/T$ only within a luminosity class (e.g. (2); (Kleinmann & Hall 1986)). Based on the temperature and luminosity range (see Table 3) we assume that the sources mostly belong to the luminosity class III and are therefore more likely giants than super giants or a mixture of classes.

The calculations were done via:

$$d = \Delta\lambda \cdot (1 - f_{min}),$$

$$EW = \int_{\lambda_1}^{\lambda_2} (1 - f_\lambda) d\lambda = \Delta\lambda \sum_{\lambda_1}^{\lambda_2} (1 - f_\lambda)$$

where f_λ is the normalized flux density in the wavelength range from $\lambda_1 = 2.2924$ to $\lambda_2 = 2.2977 \mu\text{m}$ ((2)) and $\Delta\lambda$ the wavelength bin size ($= 0.72$ nm). f_{min} is the normalized flux density of the deepest absorption in the described wavelength range.

We selected the extinguished templates ((Wallace & Hinkle 1997)) with the smallest difference in EW, bandhead depth d and apparent magnitude m_K compared to the observed spectra (see Table 3). The stellar template spectra that fit the observed ones best are shown in Fig. 6. Their physical parameters as well as the value of the K-band extinction A_K needed for the best fit are listed in Table 4.

All observed objects except IRS 5SE can be represented by late-type giants with surface temperatures in the range of $\log(T)$

Table 4. The stellar templates that best fit the observed spectra. Listed are the K-band extinction needed in the best fit and the differences of the fitted parameters between the templates and the observed sources. All but IRS 5SE can be represented by a G-type giant. See text for further comments.

Object	Stellar Type	Temp. [K]	ΔEW [nm]	Δd [nm]	Δm_K [mag]	A_K [mag]
IRS 5NE	G8III	4229	0.013	0.046	0.0	3.4
IRS 5E	G8III	4229	0.082	0.015	0.4	3.3
IRS 5S	G7III	4286	0.070	0.037	0.3	3.3
IRS 5SE	B3V	22570	0.129	0.069	1.7	2.7

$= 3.6-3.7$ (or $4000 \text{ K} < T < 5000 \text{ K}$) and with apparent K-band magnitudes of 10 to 14 mag. These values are consistent with the expected properties of stars on the AGB at the distance of the GC assuming an average K-band extinction of 3.4 mag (see also Fig. 14 in (Rafelski et al. 2007)). The only exception is IRS 5SE. From our fits we derive that for IRS 5SE the temperature is likely to be higher than 5000 K, but in this case the template stars miss to fit the observed apparent brightness by about 2 magnitudes. This is a strong indication that we observe in fact a blend of an early- and a late-type star and that the observed CO bandheads are correspondingly too weak compared to the continuum - resulting in the described discrepancies.

3.3. Spectral energy distributions, colors

In a recent paper ((Viehmann et al. 2006)), we described spectral energy distributions (SEDs) from H- to Q-band (1.6 to $19.5 \mu\text{m}$) to investigate colors, infrared excesses and extended dust emission of GC sources. The SEDs showed characteristic features. We could clearly distinguish between four types of sources (Fig. 7): the luminous northern arm bow shock sources (Type 1), the lower luminosity bow shock sources (Type 2), the cool stars (Type 3) and the hot stars (Type 4). [Note: Although the lower Type 2 source has a stronger curved short wavelength spectrum - and therefore looks more like a Type 3 source in that spectral domain - it is clearly identified as a lower luminosity bow shock source (see Viehmann et al. 2006, Clenet et al. 2004).] This classification may be used to clarify the nature of the presently unclassified sources east of IRS 5 discussed in this work. The H-, K- and L-band luminosities were derived from the comparison of IRS 13N and the sources east of IRS 5 with IRS 16NE and 16NW (m_K , H-K and K-L from (Blum et al. 1996)). For the calculations ($m = -2.5 \cdot \log(FD_{1..}/FD_{0..})$), zero flux densities from (Skinner 1997) were used ($FD_{0,H} = 1020$ Jy, $FD_{0,K} = 657$ Jy, $FD_{0,L} = 253$ Jy). The compact mid-IR sources east of IRS 5 are less luminous and situated close to or within the northern arm of the mini-spiral and therefore show similar characteristics to identified lower luminosity bow shock sources. However, with the exception of IRS 5SE, their appearance on high resolution K- and L-band NAOS/CONICA images obtained with adaptive optics does not indicate bow shock structures (see Fig. 1 and e.g. (Moultaka et al. 2004); (2005); (Viehmann et al. 2005); (Clenet et al. 2004)). Moreover, all our sources show SEDs that are either flat between 4.7 and $20 \mu\text{m}$, like the Type 2 sources of Viehmann et al. (2006) (IRS 5NE and IRS 5S, see Fig. 7), or increase towards longer wavelengths (IRS 5E, IRS 5SE1 and IRS 5SE2). This is similar to IRS 13N where a strong foreground extinction and/or dust emission ($T > 500 \text{ K}$) was assumed ((Eckart et al. 2004)). The object could be identified as a cluster of stars that heat the local environment of the mini-spiral

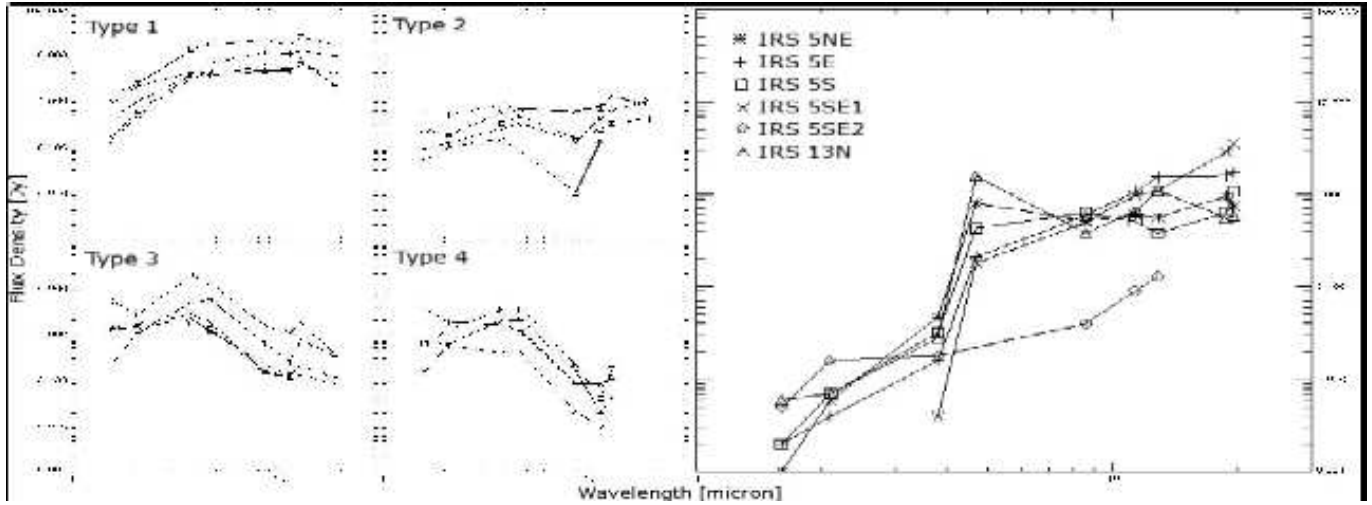


Fig. 7. The SEDs of the different types of MIR-sources introduced by Viehmann et al. (2006) compared to the five compact MIR sources located east of IRS 5 and the unclassified source IRS 13N: Type 1: luminous northern arm bow shock sources, Type 2: lower luminosity bow shock sources, Type 3: cool stars and Type 4: hot stars. For the SEDs shown in the right panel see data and error estimates in Table 2 and the corresponding caption. There is a strong onset of dust emission longward of $2.2 \mu\text{m}$ in these sources. The strongest change is present in the IRS13N sources (see Eckart et al. 2004). For sources without such a strong IR-excess (e.g. IRS 5 SE2) the transition from the non-thermal to the thermal IR is smoother.

or young stars with ages of 0.1 to 1 Myr.

The sources east of IRS 5 show very weak luminosities in H- and K-band. In the NIR two-color diagram (Fig. 8) IRS 5NE, IRS 5E and IRS 5S are located close to the positions of group II Herbig Ae/Be stars with ages of about 0.1 to 1 million yr after correction for the 30 mag of the foreground extinction. These Herbig Ae/Be stars are young stars of intermediate mass ($2-8 M_{\odot}$), embedded in dust that is not confined in disks (e.g. Hillenbrand et al. 1992)). Since the sources east of IRS 5 show similar SEDs as the IRS 13N sources and their K-band spectra are fitted by intermediate mass giants, their colors and SEDs are most probably due to the dust they are embedded in. IRS 5SE1 is less luminous in the NIR and MIR. This matches the fit of the spectrum by a giant of higher temperature than the other sources east of IRS 5.

3.4. Emission lines

The resolution in our spectra is low. Therefore we used simple Gaussian fits to derive the emission line fluxes. We list the fluxes F and line widths ν (corrected for the spectral resolution) of the detected features in Table 5. In this table, the uncertainties take into account that the $\text{Pa}\alpha$ line is located in a spectral region of lower SNR. In general, no emission lines are expected, especially if the stellar source is of late type. Therefore, a different source in the line-of-sight must be the origin of the emission lines. The gas and dust of the circum-stellar media and/or the northern arm of the mini-spiral could be responsible for all detected emission lines: the consistent average line widths suggest the same source for all emission lines.

The hydrogen recombination lines $\text{Pa}\alpha$ ($1.8756 \mu\text{m}$) and $\text{Br}\gamma$ ($2.1661 \mu\text{m}$) are the most prominent emission features in all observed spectra. Like the HeI line at $2.0587 \mu\text{m}$, they either arise in gas in the vicinity of hot early type stars or in the more extended gas distribution of the mini-spiral. In this case the gas is ionized and heated by the UV radiation field in the central parsec

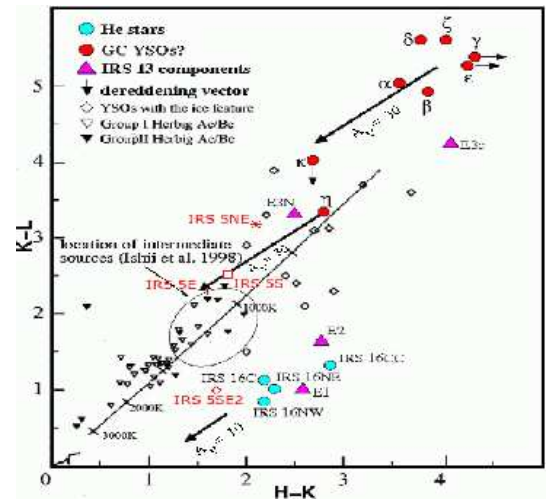


Fig. 8. HKL two-color diagram ((Eckart et al. 2004)) showing values of H-K and K-L of L-band excess sources in the IRS 13N cluster (α , β , γ , δ , ϵ , ζ , η and κ), He-stars, young stellar objects (YSOs) with ice features, Herbig Ae/Be stars of group I and II and some intermediate sources observed by Ishii et al. (1998). The locations of the sources studied in this paper are also shown. The dash-dotted line shows the colors of a single blackbody at different temperatures. An extinction vector is shown for a visual extinction of $A_V = 10 \text{ mag}$ as well as $A_V = 30 \text{ mag}$.

and therefore also linked to the presence of the massive and hot He-stars.

4. Discussion

Here we discuss the properties of the compact MIR sources east of IRS 5 based on their spectra, proper motions as well as their clustering and possible interaction with the local ISM of the GC.

Proper motions: The compact MIR excess sources close to the northern arm of the mini-spiral show proper motions to

Table 5. Fluxes and line widths (and their 1σ uncertainties) of the detected emission lines for the different observed K-band sources. The line fluxes of Br δ and Pa α suffer from atmospheric calibration problems and have to be taken with caution. For spectral flux calibration - see section 2.2.

Object	Line Feature	F $\pm\Delta$ F [10^{-19} W/m 2]	v $\pm\Delta$ v [km/s]
IRS 5NE	Pa α	551 \pm 93	400 \pm 384
	Br δ	50 \pm 8	554 \pm 370
	Br γ	50 \pm 7	356 \pm 332
IRS 5E	Pa α	649 \pm 147	390 \pm 384
	Br δ	47 \pm 9	492 \pm 370
	Br γ	87 \pm 18	357 \pm 332
IRS 5S	Pa α	649 \pm 106	490 \pm 384
	Br δ	45 \pm 7	493 \pm 370
	HeI	21 \pm 3	428 \pm 349
	Br γ	72 \pm 11	402 \pm 332
IRS 5SE	Pa α	770 \pm 176	489 \pm 384
	Br δ	96 \pm 15	508 \pm 370
	HeI	29 \pm 4	532 \pm 349
	Br γ	98 \pm 15	429 \pm 332

the east-southeast and northwest. These motions are different from the overall motion of the gas contained in the northern arm which moves predominantly southward in this section of the mini-spiral ((Paumard et al. 2006); (Muzic et al. 2007)). However, the motions of the compact sources may well be consistent with the motion of objects that are located in the clockwise and counter clockwise rotating stellar disks of the central cluster. In that case, the spatial extent of the two stellar disks would be larger than currently assumed ((Genzel et al. 2003); (Paumard et al. 2006)). The IRS 5E and IRS 5NE sources show proper motions towards the northwest. This is in agreement with the overall motion of sources in the clockwise rotating disk of stars. If the compact MIR bright objects east of IRS 5 were in interaction with the mini-spiral they would also be located behind the center of the stellar cluster - as the mini-spiral is in this region. IRS 5S1 to 3 and IRS 5SE1 show proper motions to the east-southeast. This is in agreement with the overall orientation of the counter clockwise rotating disk of stars. This stellar disk also has a higher velocity dispersion compared to the clockwise rotating disk, such that the sources could also be located behind the center of the stellar cluster. Given the width of the mini-spiral and the apparent separation and proper motion of the sources their possible interaction with the mini-spiral must still be ongoing or must have been very recent (less than a few hundred years ago).

A comparison to more luminous and well studied sources in the GC stellar cluster suggests four plausible explanations for the sources discussed here:

1. They could be young stellar objects (YSOs) which have been formed while falling into the central parts of the 0.3 pc core radius stellar cluster. These objects could be bright in the MIR since they are still surrounded by their proto-stellar dust shells or disks which are about to be lost in the dense stellar environment of the central cluster. If we find evidence for this hypothesis it will have a profound influence on the yet unsolved formation process of young stars in the central cluster.

2. They could be low luminosity counterparts of the more luminous bow shock sources (i.e. IRS 5, 10W) within the central 5".

3. They could be a more dispersed group of stars similar to the IRS 13N complex described by (Eckart et al. 2004) (Fig. 1). They are more luminous than the sources in the IRS 13N complex which may be due to the fact that they are less extinct, but show similar SEDs and colors.

4. They could be lower luminosity but dust forming AGB stars.

IRS 5NE, 5E, 5S are difficult to explain as AGB stars: Several bright ($m_K = 10$ to 12 mag) AGB stars represent both an intermediate-mass and an intermediate-age component of the GC stellar cluster with an age of about 100 Myr ((Lebofsky & Rieke 1987); (Krabbe et al. 1995); (Blum et al. 1996); (Genzel et al. 2003)). In addition to bright blue super giants (in the IRS 16 and IRS 13 complexes) and red super giants (IRS 7) these AGB stars dominate the H- and K-band images. Prominent representatives are IRS 12N, IRS 10EE and IRS 15NE.

A possible scenario is that the observed late type sources that are MIR bright and associated with dust emission are AGB stars up to 3 magnitudes fainter than their brighter representatives in the central stellar cluster (see above). Luminous and dust-enshrouded AGB stars can be found close to the tip of the AGB. They will not evolve significantly in luminosity before mass loss ends their AGB evolution. The total span of mass-loss rates which can be derived from observations reaches from 10^{-7} to 10^{-3} M_{\odot} /yr ((van Loon et al. 1999)) with typical wind velocities of the order of 10-20 km/s (e.g. (Bergeat & Chevallier 2005); (Hagen 1978)). In general, more luminous and cooler stars are found to reach higher mass-loss rates. Stellar model calculations ((Schröder et al. 2003)) show a collective mass-loss rate of 5.0×10^{-4} M_{\odot} /yr for a synthetic sample of more than 5000 brighter tip-AGB stars, which makes them excellent candidates for MIR excess emission. Also Tanner et al. (2002; see their Table 4) have pointed out that such AGB stars could be bow shock sources with winds of up to 40 km/s and appreciable stand off distances. Therefore IRS 5NE, 5E and 5S may be AGB stars and a significant amount of the MIR excess may be due to dust shells produced by the individual sources.

There are, however, indications that the sources are young:

Indications for a bow shock source near IRS 5SE: Our measurements allowed us to narrow down the stellar types of each observed source neglecting the influence of the mini-spiral. With the exception of IRS 5SE all sources show characteristics of K-type giants with $T < 5000$ K. Here, however, the reduced K-band spectrum is a composition of the spectra of the individual sources IRS SE2 and IRS SE1. IRS SE2 is blue and brighter than IRS SE1. Following the analysis of the overall spectrum of IRS 5SE in section 3.2 we therefore identify IRS 5SE2 as a hot early type star of at least spectral type B3 and attribute the CO bandhead contained in the overall spectrum of IRS SE to the fainter component IRS SE1. Due to confusion with IRS5 SE2 the CO bandhead of the western source IRS5 SE1, a cool late type star that is bright in N- and Q-bands, is diluted and therefore the stellar template we derive suggests an earlier type source. All observed sources show UV excited emission features from the gas and dust clouds they are embedded in. In all of the cases we cannot exclude that the dominant part of the hydrogen recombination lines are in fact due to emission from the mini-spiral in that region. Since the spectrum of IRS 5SE shows contributions from an early type star, and a bow shock structure is visible, superimposed on IRS 5E1, we conclude that

IRS 5SE should be classified as a lower luminosity bow shock source.

Clustering might indicate young sources: Based on their distribution and proper motion the sources associated with IRS 5NE and IRS 5SE as well as the two bright IRS 5E objects are not likely to be clustered. However, the IRS 5S1-3 objects and possibly the faint objects associated with IRS 5E1 show an indication for a clustering of the sources. Fig. 3 shows that there are at least 5 stars brighter than about $K=15$ which are located within about 250 mas of IRS 5S. Three of them show within the uncertainties, a common motion towards the east-southeast (+120 km/s in R.A. and -30 km/s in Dec.; see Table 1). This suggests that they may in fact be physically associated. Clustering of sources is apparently a frequent phenomenon in the field east of IRS 5 and in the GC stellar cluster in general (e.g. (Schödel et al. 2007); (2005); (Eckart et al. 2004); (Genzel et al. 2003)). As can be seen from Table 1 and Figs. 3 and 4 there are at least two more candidates for source clustering in the field (#14a-e and #21a-c). However, these source complexes are not as prominent in the MIR as the four sources east of IRS 5 described in this paper. Clustering of sources is usually taken as an indication of systems that are young (at least dynamically).

If the clustering of the sources and their possible association with the clockwise and counter-clockwise stellar disks is taken as an indication of youth, this is in conflict with the interpretation of IRS 5NE, IRS 5E and IRS 5S as only moderately bright AGB stars, and with their observed spectra. The location of the sources in the two-color-diagram at the position of Herbig Ae/Be group II stars also supports that the sources are young, with ages below one million years. In addition, their interaction with the mini-spiral cannot be excluded and could be a reason for their MIR brightness. This would also be fully consistent with their identification as low luminosity bow shocks from NIR/MIR SEDs. In this case, however, the CO bandheads in the spectra are difficult to explain.

5. Summary

We have presented new imaging, proper motion, and spectroscopic data on a class of compact MIR sources in the GC. The brightest sources contained in IRS 5NE, 5E and 5S may be AGB stars and a part of the MIR excess may be due to dust shells produced by the individual sources. They are, however, fainter than expected for AGB stars in the GC stellar cluster. In all cases an interaction with the mini-spiral cannot be excluded and their broad band infrared SEDs indicate that they could be lower luminosity counterparts of the identified bow shock sources, and at least in the case of IRS 5S and IRS 5E1 - may belong to dynamically young associations of stars. The blue star IRS 5SE2 is that best candidate associated with a bow shock source.

Acknowledgements. Part of this work was supported by the German *Deutsche Forschungsgemeinschaft, DFG* via grant SFB 494. K. Muzic is member of the International Max Planck Research School (IMPRS) for Radio and Infrared Astronomy at the MPIfR and the Universities of Bonn and Cologne.

References

Allen, C.W., Allen's Astrophysical Quantities, Cox, Arthur N. (Ed.), Athlone Press, London, UK, 1976 4th ed. 2000.
 Becklin, E. E.; Neugebauer, G. 1968, ApJ, 151, 145
 Becklin, E. E.; Neugebauer, G. 1969, ApJ, 157, L31

Bergeat, J.; Chevallier, L. 2005, A&A 429, 235-246
 Blum, R. D.; Sellgren, K.; Depoy, D. L. 1996, AJ, 112, 1988
 Blum, R. D.; Sellgren, K.; Depoy, D. L. 1996, ApJ, 470, 864
 Brandner, W.; Rousset, G.; Lenzen, R.; Hubin, N.; Lacombe, F.; Hofmann, R.; Moorwood, A. 2002, ESO Messenger, Vol.107, p.1
 Carr, J. S.; Sellgren, K.; Balachandran, S. C. 2000, ApJ, 530, 307
 Clenet, Y.; Rouan, D.; Gratadour, D.; Lacombe, F.; Gendron, E.; Genzel, R.; Ott, T.; Schödel, R.; Lena, P. 2004, A&A, 424, L21
 Eckart, A.; Duhoux, P. R. M. 1990, ASPC, 14, 336
 Eckart, A.; Moulata, J.; Viehmann, T.; Straubmeier, C.; Mouawad, N. 2004, ApJ 602, 760
 Eisenhauer, F.; Schödel, R.; Genzel, R.; Ott, T.; Tecza, M.; Abuter, R.; Eckart, A.; Alexander, T. 2003, ApJ, 597, 121
 Eisenhauer, F.; Genzel, R.; Alexander, T.; Abuter, R.; Paumard, T.; Ott, T.; Gilbert, A.; Gillessen, S.; Horrobin, M.; Trippe, S.; and 11 coauthors 2005, ApJ, 628, 246
 Gaffney, N. I.; Lester, D. F.; Telesco, C. M. 1993, ApJ, 407, L57
 Gaffney, N. I.; Lester, D. F.; Doppmann, G. 1995, PASP, 107, 68
 Geballe, T. R.; Rigaut, F.; Roy, J.-R.; Draine, B. T. 2004, ApJ, 602, 770
 Geballe, T. R.; Najarro, F.; Rigaut, F. et al., 2006, ApJ, 652, 370
 Genzel, R.; Schödel, R.; Ott, T.; Eisenhauer, F.; Hofmann, R.; Lehnert, M.; Eckart, A.; Alexander, T.; Sternberg, A.; Lenzen, R.; and 5 coauthors 2003, ApJ, 594, 812
 Ghez, A.M., Salim, S., Hornstein, S. D., Tanner, A., Lu, J. R., Morris, M., Becklin, E. E., Duchêne, G., 2005, ApJ 620, 744
 Gerakines, P. A.; Whittet, D. C. B.; Ehrenfreund, P.; Boogert, A. C. A.; Tielens, A. G. G. M.; Schutte, W. A.; Chiar, J. E.; van Dishoeck, E. F.; Prusti, T.; Helmich, F. P.; de Graauw, Th. 1999, ApJ, 522, 357
 Hagen, W. 1978, ApJS, 38, 1
 Hillenbrand, L. A.; Strom, S. E.; Vrba, F. J.; Keene, J. 1992, ApJ, 397, 613
 Ishii, M.; Nagata, T.; Sato, S.; Watanabe, M.; Yao, Y.; Jones, T. J. 1998, AJ, 116, 868
 Kleinmann, S. G.; Hall, D. N. B. 1986, ApJS, 62, 501
 Krabbe, A.; Genzel, R.; Eckart, A.; Najarro, F.; Lutz, D.; Cameron, M.; Kroker, H.; Tacconi-Garman, L. E.; Thatte, N.; Weitzel, L.; and 4 coauthors 1995, ApJ, 447, L95
 Lang, K. R. 1992, Astrophysical Data I. Planets and Stars, X, Springer-Verlag Berlin Heidelberg New York
 Lebofsky, M. J. 1979, AJ, 84, 324
 Lebofsky, M. J.; Rieke, G. H. 1987, AIPC, 155, 79
 Lenzen, R.; Hofmann, R.; Bizenberger, P.; Tusche, A. 1998, SPIE, 3354, 606
 Lenzen, R.; Hartung, M.; Brandner, W.; Finger, G.; Hubin, N. N.; Lacombe, F.; Lagrange, A.-M.; Lehnert, M. D.; Moorwood, A. F. M.; Mouillet, D. 2003, SPIE, 4841, 944
 Low, F. J.; Kleinmann, D. E.; Forbes, F. F.; Aumann, H. H. 1969, ApJ, 157, L97
 Martin, P. G.; Whittet, D. C. B. 1990, ApJ, 357, 113
 Menten, K.M.; Reid, M.J.; Eckart, A.; Genzel, R. 1997, ApJ, 475, L111
 Moorwood, A.; Cuby, J.-G. 1998, Msngr, 94, 7
 Moulata, J.; Eckart, A.; Viehmann, T.; Mouawad, N.; Straubmeier, C.; Ott, T.; Schödel, R. 2004, A&A, 425, 529
 Moulata, J.; Eckart, A.; Schödel, R.; Viehmann, T.; Najarro, F. 2005, A&A, 443, 163
 Muzic, K.; Eckart, A.; Schoedel, R.; Meyer, L.; Zensus, A., 2007, A&A 469, 993
 Najarro, F.; Krabbe, A.; Genzel, R.; Lutz, D.; Kudritzki, R. P.; Hillier, D. J. 1997, A&A, 325, 700
 Origlia, L.; Moorwood, A. F. M.; Oliva, E. 1993, A&A, 280, 536
 Osterbrock, D. E.; Ferland, G. J. 2006, Astrophysics of gaseous nebulae and active galactic nuclei, 2nd. ed. by D.E. Osterbrock and G.J. Ferland., Sausalito, CA: University Science Books, 2006
 Ott, T.; Eckart, A.; Genzel, R. 1999, ApJ, 523, 248
 Paumard, T.; Genzel, R.; Martins, F.; Nayakshin, S.; Beloborodov, A. M.; Levin, Y.; Trippe, S.; Eisenhauer, F.; Ott, T.; Gillessen, S.; and 4 coauthors 2006, ApJ, 643, 1011
 Rafelski, M.; Ghez, A.M.; Hornstein, S.D.; Lu, J.R.; Morris, M. 2007, ApJ, 659, 1241
 Reid, M.J.; Menten, K.M.; Genzel, R.; Ott, T.; Schödel, R.; Eckart, A. 2003, ApJ, 587, 208
 Rieke, G. H.; Lebofsky, M. J. 1985, ApJ, 288, 618
 Rieke, G. H.; Rieke, M. J.; Paul, A. E. 1989, ApJ, 336, 752
 Rigaut, F.; Geballe, T. R.; Roy, J.-R.; Draine, B. T. 2003, ANS 324, 551
 Rousset, G.; Lacombe, F.; Puget, P.; Hubin, N. N.; Gendron, E.; Conan, J.-M.; Kern, P. Y.; Madec, P.-Y.; Rabaud, D.; Mouillet, D.; and 2 coauthors 1998, SPIE, 3353, 508
 Rousset, G.; Lacombe, F.; Puget, P.; Hubin, N. N.; Gendron, E.; Fusco, T.; Arsenault, R.; Charton, J.; Feautrier, P.; Gigan, P.; Kern, P. Y.; Lagrange, A.-M.; Madec, P.-Y.; Mouillet, D.; Rabaud, D.; Rabou, P.; Stadler, E.; Zins, G.,

- 2003, SPIE, 4839, 140
- Schödel, R., Ott, T., Genzel, R., Hofmann, R., Lehnert, M., Eckart, A., Mouawad, N., Alexander, T., 2002, *Natur* 419, 694
- Schödel, R., Ott, T., Genzel, R., Eckart, A., Mouawad, N., Alexander, T., 2003, *ApJ* 596, 1015
- Schödel, R.; Eckart, A.; Iserlohe, C.; Genzel, R.; Ott, T. 2005, *ApJ*, 625, L111
- Schödel, R.; Eckart, A.; Genzel, R.; Merritt, D.; Alexander, T.; Sternberg, A.; Moultaqa, J.; Ott, T.; Straubmeier, C. 2007, *astro.ph.03178*
- Schröder, K.-P.; Wachter, A.; Winters, J. M. 2003, *A&A*, 398, 229-237
- Scoville, N. Z.; Stolovy, S. R.; Rieke, M.; Christopher, M.; Yusef-Zadeh, F. 2003, *ApJ*, 594, 294
- Skinner, C. J. 1997, *hstc.work*, 233
- Tanner, A.; Ghez, A. M.; Morris, M.; Becklin, E. E.; Cotera, A.; Ressler, M.; Werner, M.; Wizinowich, P. 2002, *ApJ*, 575, 860
- Tanner, Angelle M.; Ghez, A. M.; Morris, M.; Becklin, E. E. 2003, *ANS*, 324, 597
- Tanner, A.; Ghez, A. M.; Morris, M. R.; Christou, J. C. 2005, *ApJ*, 624, 742
- van Loon, J. Th.; Groenewegen, M. A. T.; de Koter, A.; Trams, N. R.; Waters, L. B. F. M.; Zijlstra, A. A.; Whitelock, P. A.; Loup, C. 1999, *A&A*, 351, 559-572
- Viehmann, T.; Eckart, A.; Schödel, R.; Moultaqa, J.; Straubmeier, C.; Pott, J.-U. 2005, *A&A*, 433, 117
- Viehmann, T.; Eckart, A.; Schödel, R.; Pott, J.-U.; Moultaqa, J. 2006, *ApJ*, 642, 861
- Wallace, L.; Hinkle, K. 1997, *ApJS*, 111, 445